SAE INTERNATIONAL

ARTICLE INFO
Article ID: 01-18-01-0005

doi:10.4271/01-18-01-0005

Lattice Structure and Strut Thickness Optimization for Turbine Blade Modal Parameters

Siwachai Reewarabundith[1]

[1]*Nanjing University of Aeronautics and Astronautics, China*

Abstract

This article explores the utilization of simple-cubic, diamond, octet-truss, and X-type lattice structures for low-pressure turbine blades in engine turbines to enhance natural frequency and decrease overall engine weight while maintaining structural integrity. The research method involves analyzing polylactic acid (PLA) hollow T106C blades with fully infilled and 50–80 location-based lattice arrangements. The study modifies the strut thickness of lattice structures using both constant and variable-based approaches and applies a generalized formula based on relative density to evaluate how changes in lattice thickness and arrangements influence natural frequencies. Furthermore, the investigation extends to multi-lattice configurations, introducing a parameter k to signify the transition between different lattices. The modified blades were 3D printed using PLA and tested for natural frequencies through modal testing. The results demonstrate that location-based 50–80 exponential-based lattice structures combining octet-truss and X-type lattices yield the best performance, achieving a 15% increase in the first mode and 14.6% in the second mode when compared to hollow blade. In comparison, fully infilled 50–80 exponential-based lattice structures with a combination of octet-truss and X-type lattices achieve a 9.4% increase in the first mode and 12.7% in the second mode. These findings highlight that lattice structures can effectively improve natural frequencies across all modes.

History

Received: 20 Aug 2024
Revised: 24 Dec 2024
Accepted: 24 Jan 2025
e-Available: 07 Feb 2025

Keywords

Simple-cubic, Diamond, Octet-truss, X-type lattice, Natural frequencies, Low-pressure turbines (LPT), Experimental modal analysis

Citation

Reewarabundith, S., "Lattice Structure and Strut Thickness Optimization for Turbine Blade Modal Parameters," *SAE Int. J. Aerosp.* 18(1):57-74, 2025, doi:10.4271/01-18-01-0005.

ISSN: 1946-3855
e-ISSN: 1946-3901

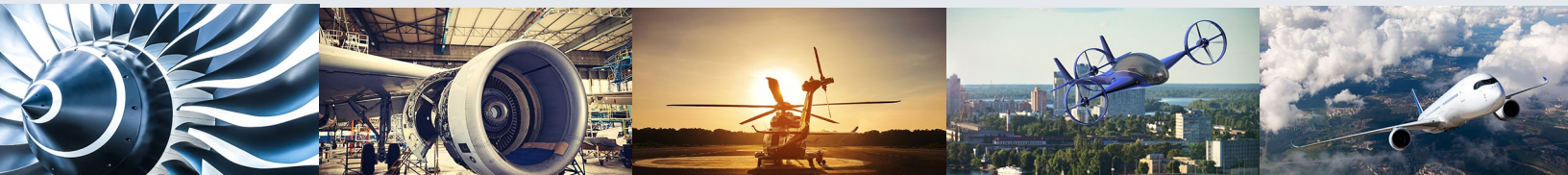

1. Introduction

Aircraft turbines consist of two stages: high-pressure and low-pressure turbine (LPT) stage. The LPT in a large, high-bypass ratio engine serves the crucial role of supplying power to drive the fan. In some cases, it also contributes to driving a few compressor stages. The turbine must operate at a low rotational speed, matching the fan speed [1]. Additionally, the presence of the bypass duct limits the outer diameter of the LPT. This combination of low rotational speed and restricted diameter results in blade speeds typically equivalent to Mach numbers ranging from approximately 0.4 to 0.7 [2].

The LPT is also heavy and costly. However, improving its polytropic efficiency by just 1% can lead to a significant improvement in fuel consumption, typically ranging from 0.5% to 1.0%, thus increasing the distance an aircraft can travel [3]. Achieving better engine efficiency requires higher turbine inlet temperatures. Yet, this presents challenges, as turbine blades must operate for extended periods at temperatures that exceed their melting points. These challenges include high centrifugal stress, reduced rigidity, and exposure to high-speed Mach number flows, oxidation, inter-diffusion, and centrifugal forces generated by high-speed rotation [4]. As a result, turbine blade materials must exhibit excellent creep resistance and effective cooling capabilities. Nickel alloys are commonly used to construct turbine blades and nozzle guide vanes due to their favorable high-temperature properties. Additionally, ceramic thermal barrier coatings are applied to enhance the performance of turbine engines in both propulsion and power generation. These coatings act as a refractory insulation, allowing engines to operate at higher temperatures while reducing the harmful effects on the metal components.

Despite extensive research efforts conducted over the past 15 years, the efficiency of LPTs has exhibited minimal improvements, regardless of variations in stage loading or flow coefficient or using improved materials. With current state-of-the-art turbine efficiency levels already exceeding 90%, research in improving this section is primarily challenging to achieve. Consequently, the study now mainly focuses on improving engine design and efficiency through the weight reduction of LPT. The LPT accounts for approximately 25%–30% of the engine's total mass and 15% of the total engine costs. A NASA study has shown that a 10% reduction in the weight of the LPT is proven to be more effective than reducing the weight of other engine component based on the direct operating cost plus interest (DOC+I) of an engine on a large transport aircraft [5].

Researchers have used various techniques to decrease the weight of the LPT. A particularly underrepresented area in the literature is the application and study of high-lift profiles. The term "high-lift" inherently implies increased loading, a sought-after attribute in the gas turbine industry. High-lift designs hold the potential for reducing blade numbers by extracting more work per blade, consequently demanding fewer blades to achieve the same overall power extraction.

Due to the high-lift profile, there will be an aggravation in the separation and transition effects on the blade's suction surface due to increased adverse pressure gradients. This separation will induce forced vibrations onto the blades [6]. The two common types of vibration include flutter and buffeting. Buffeting is an unsteady aerodynamic force that occurs when the airflow over an airfoil separates due to oscillatory pressure fluctuations on the airfoil's surface, which induces vibrations. The resulting adverse solid pressure gradient at the separation of the boundary layer on the suction side of the blades, particularly at a low Reynolds number, causes a significant loss in lift and a consequent drop in the engine [7]. Flutter is a self-excited vibration known to be more severe and potentially catastrophic due to the interaction of aerodynamic forces, structural dynamics, and the airflow over the blades. It typically manifests at frequencies near a blade mode frequency because structural forces predominantly influence the vibration frequency.

Other types of vibration include rotor–stator interaction. Interaction between the rotating rotor blades and stationary stator vanes can cause dynamic forces and vibrations, particularly at the rotor–stator interface [8]. The casing perceives the constant force's rotation around the engine axis as a fluctuating force that changes over time, oscillating at a frequency equivalent to the rotational speed [9]. Therefore, a methodology in this research is implemented through the usage of lattice structures to increase all modes of natural frequency of the high-lift blades, effectively reducing the vibrations. To incorporate lattice structures effectively in high-lift blades, it is essential to optimize their configuration to enhance the blade's natural frequency and reduce vibrations. By understanding the mechanical behavior of different lattice structures, we can tailor their design to achieve the desired mechanical properties.

Lattice structures are complex three-dimensional configurations with a well-defined topology of one or more repeating unit cells. These unit cells, characterized by the dimensions and interconnections of their constituent strut elements, are linked at specific nodes [10]. Gibson et al. defined lattice structures as cellular material consisting of "an interconnected network of struts or plates" [11]. Ashby et al. further stated that lattice structures, a form of cellular material, differ from large-scale engineered structures such as trusses or frames in terms of their scale—the unit cells of a lattice structure have a millimeter or micrometer scale [12]. Adjusting various parameters of lattice structures, such as cell topology, interconnections, or geometry, can significantly modify their physical properties, enabling them to demonstrate unique characteristics not achievable by the materials from their initial form. These properties include acoustic, dielectric, and mechanical attributes [13].

Lattice structures are classified according to their mechanical behavior, falling into two main categories: those primarily governed by bending behavior and those primarily dominated by stretching behavior. Bending-dominated structures, such as diamond and X-type, tend to undergo bending moments within their structure, making them more flexible or compliant. In contrast, stretch-dominated structures, such as simple-cubic and octet-truss, experience axial loads, making them stiffer and more robust than their bending-dominated counterparts. The lattice structure used within the high-lift blade includes simple-cubic, diamond, X-type, and octet-truss lattices shown in Figure 1. Simple-cubic structure features a lone lattice point situated at each corner of the unit cell, which has the shape of a cube, fitted for structures that are able to withstand a large load in a single direction [14]. The diamond unit cell can be defined as an isotropic configuration composed of four struts that are nodally connected to another four struts. This unit cell possesses isotropic geometry, with each connection node of the struts resembling a tetrahedron and being surrounded by four other connection nodes [15]. The octet-truss lattice structure features a nodal connectivity of 12 and exhibits an almost isotropic yield surface. When constructed using materials with high specific strength, the octet-truss lattice becomes an extremely weight-efficient structure capable of supporting multiaxial stress. Its stiffness and strength exhibit linear scaling in relation to the lattice's relative density. Octet-truss lattices are mechanically suitable to support loads in multiple directions [16]. X-type lattice structures are organized to form a pattern that resembles the letter "X" when viewed in three dimensions. Its advantages include a high strength-to-weight ratio and the ability to support heavy loads while remaining relatively lightweight, making them ideal for applications where weight efficiency is crucial, such as aerospace applications [17].

The high-lift blade used for the implementation of four different lattice structures in the research is the T106C blade. The T106C blade is a mid-loaded and high-lift blade, which is the modified version of the original T106 blade created by Motoren-und Turbinen-Union (MTU) Aero Engine, characterized by an increased pitch-to-chord ratio of 0.799–0.95. The parameters of the blades are shown in Table 1. The T106C blade model is also available as an IGES/step CAD file constructed from the dimensions and coordinates provided by R. Stieger [18].

TABLE 1 T106C blade characteristics.

Parameters	Values	Units
Chord	93.01	mm
Blade height	225	mm
Pitch-to-chord ratio	0.95	-
Aspect ratio	2.4	-
Throat	43.38	mm
Blade stagger angle	30.7	deg
Inlet flow angle	32.7	-
Zweifel coefficient	1.29	-

2. Blade Design

The T106C blade is strategically implemented with a complete cavity design extending from the base to the blade's tip using topology optimization shown in Figure 2. The topology optimization performed on the T106C blade focused primarily on volume reduction boundary conditions, a methodology that has yielded favorable results in previous studies, such as that by Antorkas [19]. Antorkas et al. did the topology optimization for 50% volume reduction T106C blade and concluded that removing a portion over the chord line from 10% to 65% and 85% to 95% from root to 90% of the blade span but introduces a weight at the tip of the blade similar to a lump mass system. This lump mass would create unwanted vibration so a decision is made by carving the blade into a fully hollow blade, located from 10% to 65% on the camber line across the whole span length, occupying 90% of the total weight of the blade.

From Table 2, when compared with the original T106C blade, the modified blade presents a huge weight reduction in the overall weight, but it also reduces the natural frequency of the blade itself; therefore, fully infilled and

FIGURE 1 Geometry of the T106C: (a) simple-cubic, (b) diamond, (c) octet-truss lattices, and (d) X-type.

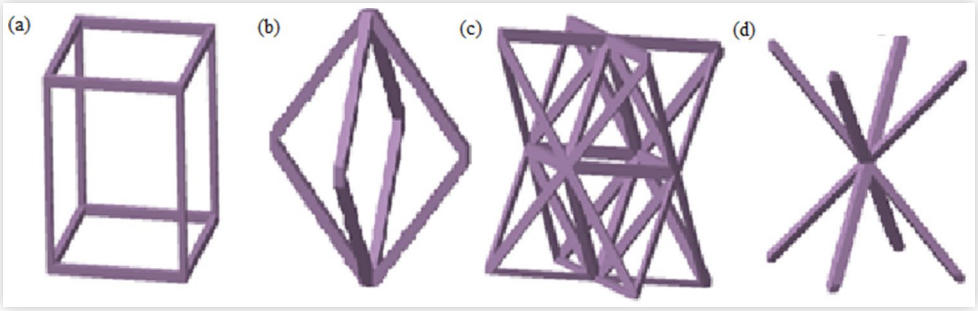

FIGURE 2 Geometry and dimensions of hollow T106C high-lift blade.

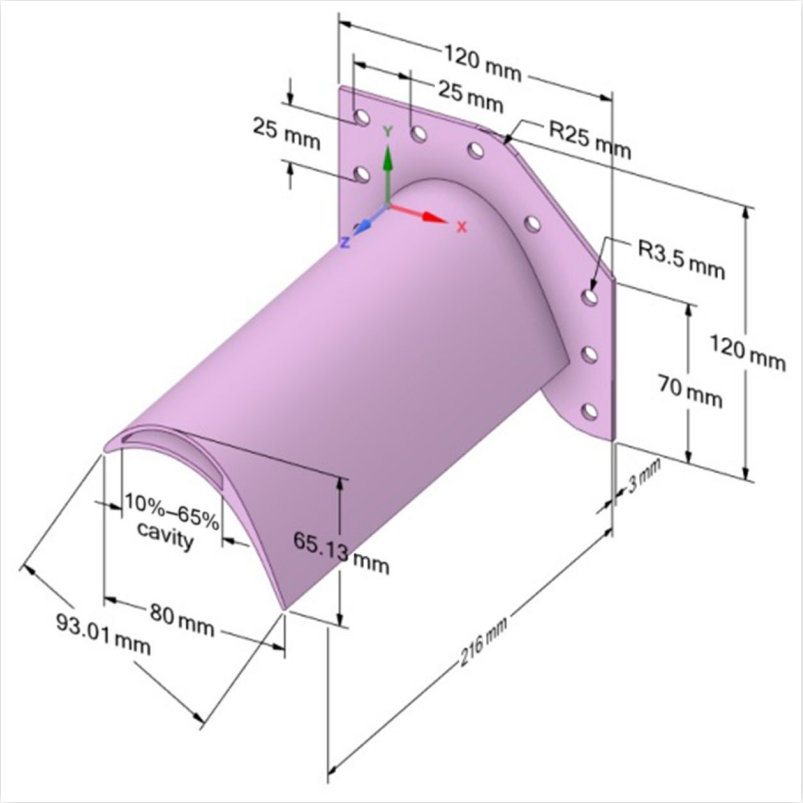

50–80 location-based designs are the two types of lattice arrangements used in this research to increase the natural frequency shown in Figure 3. Lattice structures fully occupy the cavity space for a fully filled design, and a single-based row lattice occupies 50% and 80% point of the cavity space in the 50–80 location-based and is designed using CATIA V5 software.

Using the strategic position given, the lattice structures are given the initial parameters in which the cell dimensions for each type of lattices are fixed at a constant of 9.5 mm × 9.5 mm × 9.5 mm and the length of the blade is set as a constant of 216 mm. This study develops lattice structures for turbine blades through a systematic process that uses manual tuning with optimization principles inspired by methods such as genetic algorithm (GA). A series of blade models with uniform strut thicknesses are generated by varying the thickness in increments of 0.1 mm, ranging from 0 mm, which represents the hollow blade, up to 2 mm. This allows for the analysis of how different thickness values affect the blade's natural frequencies and overall performance. The results of each mode of natural frequencies are plotted and the optimal thickness values are identified using a best-fit curve.

TABLE 2 Comparison of PLA T106C solid and hollow blade.

Lattices	Frequency mode			
Types	Mode 1	Mode 2	Mode 3	Mass (kg)
Solid	75.037	147.01	259.44	0.23448
Hollow	79.191	143.17	260.15	0.15414

The study then extends to variable lattice designs, where strut thickness is adjusted across different regions of the blade. The relative density formula determines the variable thickness throughout the lattice structure. This approach allowed for the creation of a lattice design where the strut thickness varied in response to the density requirements. This method aimed to enhance natural frequencies further by tailoring the lattice geometry to more precisely meet the performance criteria. This approach further optimizes natural frequencies by tailoring the lattice geometry to the specific density requirements of each region. The variable thickness lattice model is developed based on the optimal thickness obtained from the uniform lattice designs and then subjected to finite element analysis to evaluate its modal characteristics, comparing the results against the initial constant thickness designs to verify improvements in natural frequencies and other modal parameters.

The investigation then expanded to multi-lattices, introducing a specified parameter k, which signifies the transition between two lattice structures. This parameter controls the gradient and transition smoothness from one lattice type to another. By carefully adjusting k, regions of the blade can be designed with different lattice types that best meet local performance requirements.

FIGURE 3 50–80 location-based design (left) and fully infilled design (right).

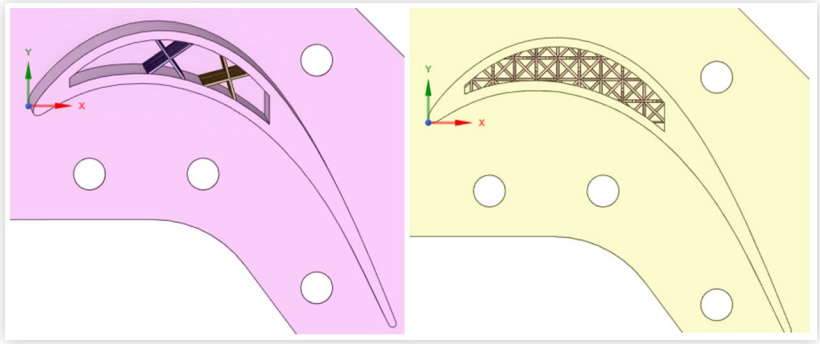

Different multi-lattice configurations are analyzed, including combinations such as simple-cubic with diamond, octet-truss with X-type, and other permutations of lattice structures, thereby maximizing structural integrity and performance.

Lastly, experimental verification of the 3D-printed blades is conducted using polylactic acid (PLA) material. Operational frequencies observed in LPT, operating between 2500 rpm and 10,000 rpm, have corresponding frequencies in the range of 40–166 Hz. To avoid resonance and ensure safe operation, the first natural frequency of the blade must be 1.5–2 times higher than this range. For composite materials, their higher stiffness inherently results in higher natural frequencies. Materials such as U-500 and IN738 push the natural frequencies well beyond 2 times the resonant frequencies for the same geometries and configurations. This characteristic makes composite materials particularly well-suited for turbine blade applications. The incorporation of lattice structures further enhances natural frequencies by increasing stiffness without adding significant mass. For example, employing a constant full X-type lattice structure in a composite blade increased the first natural frequency to 505 Hz, a 6.1% improvement compared to the hollow blade design (476 Hz). This highlights the combined effect of composite materials and optimized lattice configurations in achieving exceptional vibrational performance. Although composite materials are used in real-world blades, PLA is chosen for cost efficiency as the research primarily focuses on the effect of lattice structures and how their thickness influences the natural frequency of the blades. PLA has a lower printing temperature and is less likely to warp. Table 3 shows the mechanical properties of PLA material used in the computational and experimental analysis. This approach allows for assessing vibrational characteristics for computational model validation, paving the way for advanced testing in the future.

TABLE 3 PLA mechanical properties.

Properties	Value	Units
Density	1250	kg/m^3
Young's modulus	2.2	GPa
Poisson's ratio	0.3	-
Bulk modulus	1.8333	GPa
Shear modulus	0.84615	GPa

While the optimization process was performed manually, it is conceptually similar to optimization algorithms such as GA, where different solutions are systematically explored, evaluated, and refined. By iterating through various design options and combining the best features from constant and variable thickness designs, the study creates multi-lattice structures that balance strength, stiffness, and vibrational properties for optimal turbine blade performance. Also, the lack of comprehensive research on high-lift profiles is notable; often overlook the complex dynamics associated with high-lift profiles especially considering their potential impact on natural frequency and vibrations. This study aims to fill this research gap by focusing specifically on high-lift profiles. This approach provides a new direction for future advancements in turbine blade design, contributing to more efficient and cost-effective aircraft engines. The application of these findings can lead to substantial improvements in the aviation industry's operational efficiency and environmental impact.

3. Constant Lattices

We employed a systematic approach using each model design's strut thickness range to conduct the constant lattice design and analysis. This comprehensive exploration involved multiple iterations of strut thicknesses ranging from 0 mm to 2 mm for each lattice variant, with thickness values drawn in intervals of 0.1 mm. This approach ensured a robust and detailed dataset for thorough analysis. Two types of lattice arrangements, fully infilled and 50–80 location-based, are being used. All four lattice variants including simple-cubic, diamond, X-type, and octet-truss lattices are being drawn individually in CATIA to ensure the accuracy of lattices within the blade. The file is uploaded to ANSYS software, where

FIGURE 4 Constant thickness variation lattices graph.

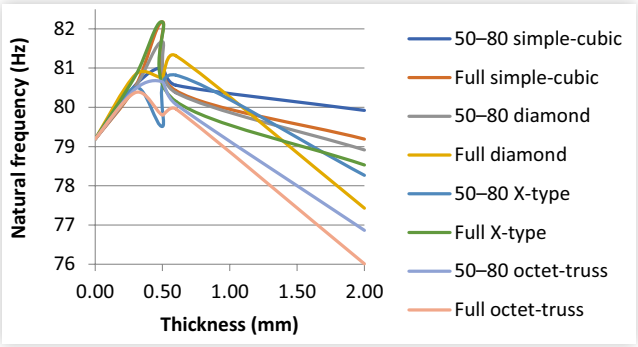

tetrahedron meshing is used for the blade's finite element analysis. The natural frequency of each lattice structure was calculated and the eight results can be concluded and are drawn in the natural frequency versus thickness graph shown in Figure 4.

The graph findings depicted in Figure 4 shows the first natural frequency of specific lattice structures, notably the full X-type and full simple-cubic, experiences a notable upswing as the strut thickness increases up to 0.5 mm, with specific lattice types, notably 50–80 X-type and full octet-truss, witnessing a pronounced decrease during this phase. However, beyond the 0.5 mm threshold, an overall decreasing trend in the first natural frequency is observed. The relationship between the first natural frequency behavior of lattice structures and changes in thickness unfolds through several vital mechanisms. As lattice thickness increases, the structure stiffens due to more excellent resistance to deformation from the increased material. A critical point is reached at approximately 0.5 mm strut thickness, triggering a transitional behavior where the dominance of stiffness escalation over mass distribution results in a sudden, sharp increase in first natural frequency. Material properties also contribute significantly, with different materials exhibiting varied responses to thickness changes. Following the 0.5 mm threshold, a shift occurs. Beyond this point, increasing thickness yields diminishing returns in terms of stiffness, and the added material contributes more to mass than stiffness resulting in a decrease in first natural frequency. From Table 4, we can find the results of lattice structures with thickness of 0.5 mm, which has the highest natural frequency. The last column represents the percentage difference of first mode frequency compared with the hollow blade.

Whereas for the higher modes of frequency in constant lattices, there is a 10% slight increase in the second mode of frequency shown in numerical results recorded in Table 4. 50–80 X-type lattices produce the highest second natural frequency. This shows that the lattice structures show improvement in resisting the torsional vibration than conventional turbine blades. In contrast to the second mode, the frequencies of higher modes (third mode and above) exhibit minimal change. This suggests that the structural characteristics governing the higher modes remain relatively consistent or less affected by variations in lattice parameters. For the third mode of frequency, 50–80 X-type and octet-truss lattices show the most significant increase in natural frequency while others remain relatively constant.

In this section, we analyzed a wide range of thicknesses for a constant lattice design and found that the lattice structure with a 0.5 mm thickness contributes to the highest natural frequency. This particular thickness represents a critical transition point where changes in stiffness and mass distribution significantly impact the natural frequency of all the designed lattice structures. The mass and volume are being recorded to be established as a baseline for variable thickness design in the next section (see Table 5). From this design with a constant thickness, we observe that the first natural frequency increases significantly with the addition of lattices, while higher-order natural frequencies show only a minimal increase and remain relatively constant. From the constant thickness design, we observe that the first natural frequency increases significantly with the addition of lattice material, while higher-order natural frequencies show only a minimal increase and remain relatively constant. This suggests that using a constant lattice thickness is insufficient for meeting the research objectives. Therefore, a second approach is introduced by using relative density. By using the data in which lattice thickness is kept constant at 0.5 mm, we can obtain the density for each lattice variant and further understand

TABLE 4 Natural frequency of uniform lattice structures (0.5 mm).

Lattices		Frequency mode			
Types	Configuration	Mode 1	Mode 2	Mode 3	1st mode freq. diff.
Simple-cubic	Fully filled	82.179	160.57	260.78	3.77%
	50–80	81.014	167.30	269.70	2.30%
Diamond	Fully filled	80.774	166.76	267.01	2.00%
	50–80	81.673	160.74	260.36	3.13%
Octet-truss	Fully filled	79.801	166.72	267.95	0.77%
	50–80	80.647	167.08	269.12	1.84%
X-type	Fully filled	82.174	164.41	265.71	3.77%
	50–80	80.439	167.25	269.17	1.58%

TABLE 5 Mass and volume design lattices blade (0.5 mm thickness).

Types	Configuration	Total volume V_T	Volume of lattices V^*	Mass (kg)
Hollow	-	123,310	-	0.15414
Simple-cubic	Fully filled	123,690	380	0.15462
	50–80	123,430	120	0.15429
Diamond	Fully filled	124,170	860	0.15521
	50–80	123,710	400	0.15464
Octet-truss	Fully filled	126,020	2710	0.15752
	50–80	124,730	1420	0.15592
X-type	Fully filled	125,220	1910	0.15653
	50–80	123,920	610	0.15490

how changes in thickness, while maintaining constant relative density, influence the mechanical behavior of the lattice.

4. Gradient Lattices

The effect of thickness variation is also another important factor in how it will affect the natural frequency. From the previous section, increasing the strut thickness increases the stiffness, therefore enhancing the natural frequency of the blade. However, this comes with an increase in the overall mass of the object which also reduces the natural frequency. With these facts mentioned, it is a requirement to optimize the thickness of lattices struts to strike a balance between them and ensure that the model would produce a maximum natural frequency in all modes.

In every lattice cell, the thickness struts will vary in the thickness. The top layer of the structure has the lowest density or is also known to have the smallest strut size, which increases gradually throughout the layer, forming the highest density in the bottom part of the structure. Since the research focuses on the thickness of the struts, the mean relative density is a controlled variable used to determine the thickness. It is kept constant for both constant and gradient-based lattice structures by independently setting a target relative density for each lattice type, which can be obtained from the designed constant lattices, and then optimizing the variable-based thickness of each lattice type to achieve the desired relative density. This approach allows for flexibility in design, as it recognizes that different lattice structures may require different thickness distributions to achieve their specified relative density.

We can define an algorithm or formula to calculate the optimal strut thickness for each variable strut thickness design based on relative density. Relative density ρ is defined as the proportion of the lattice structure's density ρ^* to that of the constituent material ρ_s, which is equivalent to the volume fraction of the lattice structure V^* relative to the cavity space V_s:

$$\rho = \frac{\rho^*}{\rho_s} = \frac{V^*}{V_s} \tag{1}$$

Since the variable-based lattice structures are characterized by varying strut thickness along the length of the blade, the total volume can be further expressed in terms of the summation of the volume of lattice cells in each section of a blade, where each section has its own specific strut thickness:

$$\rho_{uniform} = \rho_{variable} = \sum_{i=1}^{n} \rho_i = \sum_{i=1}^{n} \frac{V_i^*}{V_s} \tag{2}$$

Each section of the blade contains multiple lattice cells, and it is more efficient to calculate the volume of each lattice cell within its respective section. Since the cell size is kept constant as an initial parameter, we can determine how many lattice cells each section occupies. To determine the volume occupied by each lattice cell with the same thickness, we can derive a general formula for the volume of a lattice cell by considering the dimensions and arrangement of the struts within the cell. In section i of a blade, a lattice cell is composed of multiple lattice struts, which can be represented as a rectangular beam:

$$V_i^* = t^2 L_T \tag{3}$$

where t is strut thickness and L_T is the length of the struts. Within each lattice cell, the struts intersect, leading to variations not only in thickness but also in length. We further extend the equation to account for these variations in both strut thickness and length:

$$L_T = a_1 L + a_2 l + a_3 l + b\sqrt{2}l + c\sqrt{3}l \tag{4}$$

where L is the length of a lattice cell, also known as the cell size that is kept as initial parameter, l is the total length of a lattice cell minus the thickness of the struts on both ends due to the intersection, a_1 and a_2 are the number of

FIGURE 5 Strut-based formula representation.

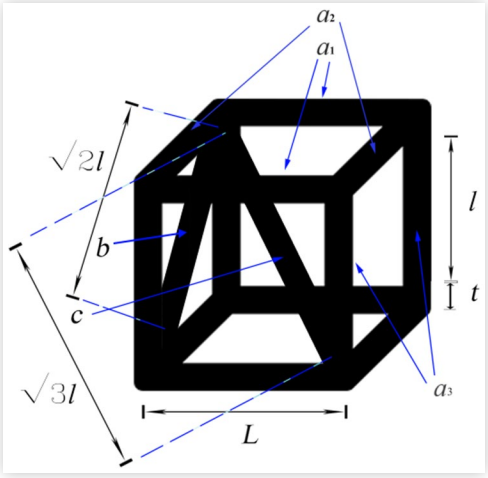

horizontal and vertical struts in the top and bottom views of a single-lattice cell; a_3 is the total number of vertical struts in front, back, and side views; b is the total number of diagonal struts on all faces; and c is the number of diagonal members across the canter of the lattice cell. Taking a simple-cubic as an example, Equation 4 and its variable can be represented in the form of an image for easier understanding (see Figure 5).

Furthermore, when individual lattices are connected, they share some of the struts together. To prevent the overlapping of lattice cells from causing excessive volume measurement error, we must account for the shared features. We further define the cross-sectional area of each strut. a_1, a_2, and a_3 have a cross-sectional area represented by a quarter of the rectangular beam as the struts share with three other cells, b has a half cross-sectional area as it only shares where the faces of the cell are connected to, and c has a full cross-sectional area as it does not share with any cells. We can find that the volume of a lattice cell is:

$$V = t^2\left(\frac{a_1 L}{4} + \frac{a_2 l}{4} + \frac{a_3 l}{4} + \frac{b\sqrt{2}l}{2} + c\sqrt{3}l\right) - (c-1)e_c \quad (5)$$

where e_c is the intersecting volume of struts c at the middle of the cell that has a thickness t. From this equation, we have derived the generalized equation for the volume of a single-lattice cell, by simply counting the number of struts within a given lattice design. Since the volume formula of Equation 5 applies to a single-lattice cell, we need to consider the volume of the particular section as shown in Equation 6:

$$V^* = \left(\frac{216}{nL}\right)\left(\frac{44}{L}\right)t^2\left(\frac{a_1 L}{4} + \frac{a_2 l}{4} + \frac{a_3 l}{4} + \frac{b\sqrt{2}l}{2} + c\sqrt{3}l\right) - (c-1)e_c \quad (6)$$

The width and length of the cavity are 44 mm and 216 mm, respectively, where n is the number of sections cut along the span-wise direction. From this addition to the equation, we can find the number of lattice cells within the section. Another important factor is the restricted height of the lattice cells due to the blade's cavity. Since the cell size in this research is bigger than the blade's cavity, there is a need to consider the geometry of the blade as the boundary constraint as it affects a_3. This means that the length a_3 is no longer length l and is denoted with a new variable d. By doing this, we can reduce the error of the theoretical and computational results. By denoting d as the distance calculated between the top surface and the bottom surface of the blade's cavity, we can establish a Bezier curve using three control points in the form of

$$P = (1-u^2)P_1 + 2(1-u)uP_2 + u^2P_3 \quad (7)$$

where u is the ratio percentage where the lattices are located. The domain is set for $x \in (8,52)$, which is defined based on the Cartesian coordinate system derived from the blade shape in CATIA, with the origin (0,0) placed at the tip and the leading edge of the blade. The domain is defined to represent the cavity space between 10% and 65% of the chord length, projected in the z-direction, which is essential for calculating the cavity height. We can obtain the control points from CATIA to write out the Bezier curves for both surfaces of the cavity (shown in Figure 6):

$$F(u) = (1-u^2)(8,8.199) + 2(1-u)u(31.799,26.881) + u^2(52,4.31) \quad (8)$$

$$G(u) = (1-u^2)(8,6.259) + 2(1-u)u(32.357,14.784) + u^2(52,-1.974) \quad (9)$$

FIGURE 6 Bezier curve of cavity space.

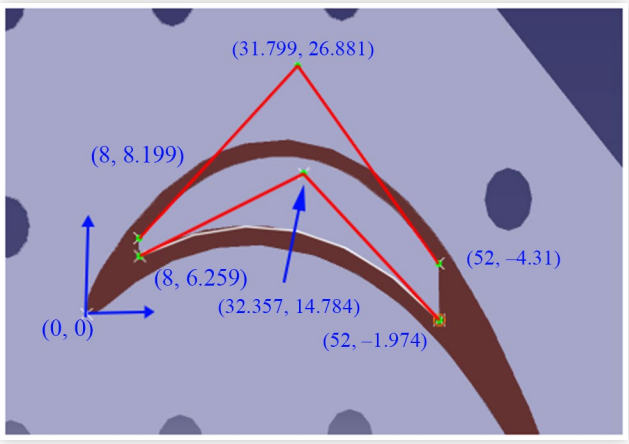

A clear illustration of the Bezier curves is shown above in respect to the cavity space. Therefore, we can obtain the corresponding height at a particular point in cavity space.

$$d = \sqrt{\left(x_F - x_G\right)^2 + \left(y_F - y_G\right)^2} \tag{10}$$

where x and y are the Cartesian coordinates and the subscript corresponding to the curve equation. Since d affects the length of a_3, the l of a_3 is replaced by d to form a_3d. Then by substituting Equation 6 into Equation 2, the mean relative density is shown below:

$$\rho = \frac{\sum_{i=1}^{n}\left\{\left(\frac{216}{nL}\right)\left(\frac{44}{L}\right)\left[t^2\left(\frac{a_1L}{4}+\frac{a_2l}{4}+\frac{a_3d}{4}+\frac{b\sqrt{2}l}{2}+c\sqrt{3}l\right)-\left(c-1\right)e_c\right]\right\}_i}{64{,}270} \tag{11}$$

The constant variable V_s is the cavity volume of the blade, which is equivalent to 64,270 mm^3. The formula can be adjusted for each type of configuration by changing the values of variables a_1, a_2, a_3, b, and c. To ensure that the formula is accurate, the comparison of ANSYS and theoretical results of constant lattices are being established shown in Table 6. From the calculation and numerical results from ANSYS software, the percentage difference is within 5% showing that the formula is accurate enough within the suitable range. The error is due to the complex intersection within the lattice cells that are being simplified in the formula, and the intersection between the lattices and the blades can only be approximated to avoid the over-complexity of the formula. This formula can then be used to control the relative density for constant and gradient-based lattices so that we can focus on the strut thickness variation of the lattices, which is the main purpose of this research. The formula can be used to calculate the suitable strut thickness of each variable thickness based on how the blade can be designed, whether it involves dividing the blade into equal sections or adhering to a specific function.

4.1. Discrete Thickness

The blade can be divided in many sections with different thickness. For example, from the general formula derived above, substitute $n = 2$. Let the thickness at base section as $2t$ and section of the tip of blade as t, using the generalized relative density formula, the calculated thickness is 0.3 mm and 0.6 mm for tip and root of the blade (see Figure 7). Likewise, we can do for three sections or more.

4.2. Gradient Thickness

Moreover, if using a linear or exponential function is used to represent the thickness of lattice, we can understand that the blade is cut into very small sections, with thickness increasing from top to bottom along the span-wise direction of the blade. Implementing the formula, we can substitute in the values in which n is the maximum number of lattice rows, the calculated maximum and minimum thickness of the lattices is 0.3 mm and 0.6 mm, respectively, and the equation of linear-based span-wise function can be represented simply as:

$$y = -\frac{t}{216}x + 2t = -\frac{0.3}{216}x + 0.6 \tag{12}$$

For an exponential-based thickness, the function used for the blade where the minimum and maximum thickness is 0.1 mm and 4 mm, respectively (see Figure 8).

$$y = 2\left(0.98\right)^x \tag{13}$$

4.3. Gradient-Based Lattice Results

The specific design choice of linearly decreasing the thickness of blades while increasing the number of sections is expected to exhibit an impact on the vibration modes of the structure. Notably, the first mode of vibration may experience minimal alteration, suggesting that the fundamental frequency remains relatively unaffected by this specific design variation (see Figure 9).

TABLE 6 Comparison of CAD and theoretical relative density.

Lattices		Volume		Relative density (%)		
Types	Configuration	Numerical	Theory	Numerical	Theory	Diff.
Simple-cubic	Fully filled	380	385.95	0.59	0.6	0.59%
	50–80	120	123.22	0.19	0.2	0.52%
Diamond	Fully filled	860	856.70	1.34	1.33	0.74%
	50–80	400	393.65	0.62	0.61	1.61%
Octet-truss	Fully filled	2720	2740.69	0.42	0.43	0.24%
	50–80	1420	1377.07	2.22	2.14	3.60%
X-type	Fully filled	1910	1919.65	2.97	2.99	0.67%
	50–80	610	632.74	0.95	0.98	3.06%

FIGURE 7 Double section of full simple-cubic.

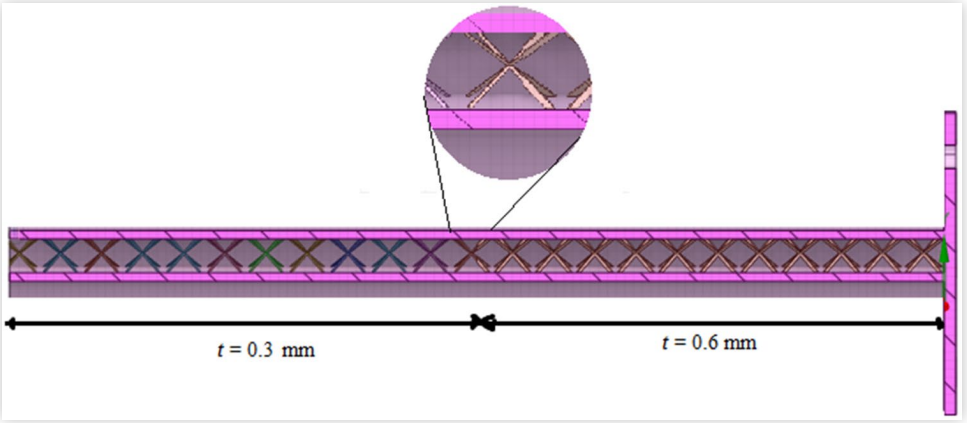

FIGURE 8 Exponential-based of 50–80 octet-truss.

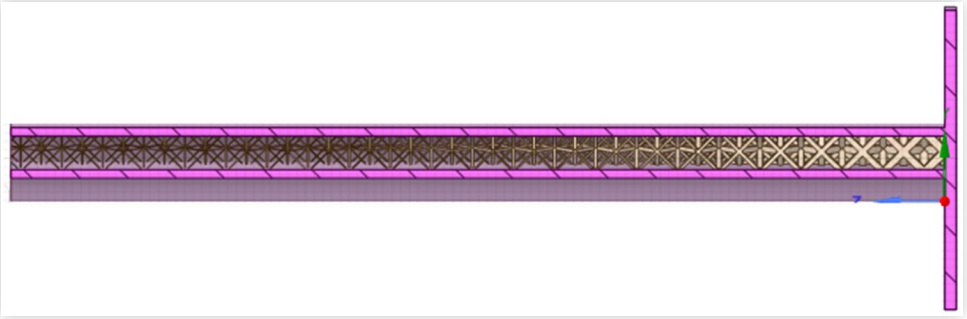

FIGURE 9 Section-based thickness variation of gradient lattices.

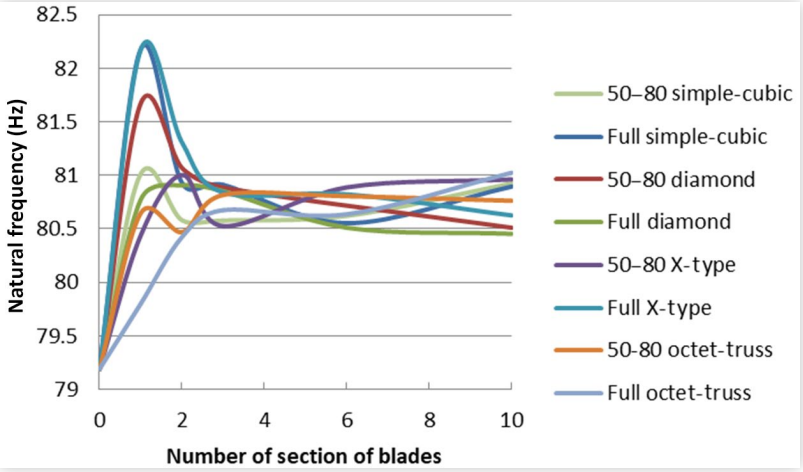

This is because the first natural frequency primarily depends on the overall stiffness of the structure rather than its mass distribution. An increase in the number of sections compensates for the reduction in thickness, maintaining the overall stiffness of the structure. As a result, the fundamental frequency, which is primarily governed by the structure's stiffness, remains relatively unaffected by this specific design variation. However, a discernible increase in natural frequency is observed for the second and third modes of vibration. This observed behavior in higher modes can be attributed to the redistribution of mass and stiffness along the blades. As the number of sections increases, the exponential decrease in thickness contributes to a more distributed mass and altered stiffness profile, particularly affecting the structural response in higher vibrational modes. The redistribution of these mechanical properties plays a significant role in influencing the dynamic behavior of the structure, resulting in an increase in natural frequencies for modes beyond the fundamental.

Another interesting factor is when it comes to increasing or decreasing the gradient of the function based on span length, as we increase the gradient constant, the natural frequency will increase similar to the results in the table as the configuration changes from linear-based to exponential-based (see Table 7). The 50–50 and 30–30–30 configuration refers to a blade divided into two and three equal sections, respectively, each with a different thickness. The linear configuration involves a gradual, uniform change in thickness from the tip of the blade to the base, where the thickness varies linearly along its length. Lastly, the exponential configuration features a nonuniform, exponential change in thickness from the tip to the base, leading to a more significant variation in thickness as you move along the blade's length. The increase in natural frequency is due to the

TABLE 7 Natural frequency of gradient-based lattice structures.

Lattices			Frequency mode				
Types	Configuration	Thickness profile	Mode 1	Mode 2	Mode 3	Mass (kg)	1st mode freq. diff.
Simple-cubic	50–80	50–50	80.581	167.33	269.28	0.15427	1.76%
		30–30–30	80.579	167.33	269.28	0.15427	1.75%
		Linear	80.924	166.81	269.38	0.15426	2.19%
		Exponential	80.741	167.74	269.41	0.15474	1.95%
	Fully filled	50–50	80.929	166.71	269.17	0.15458	2.19%
		30–30–30	80.911	166.66	269.13	0.15451	2.17%
		Linear	80.896	166.66	269.14	0.15454	2.15%
		Exponential	81.025	168.56	270.05	0.15614	2.32%
Diamond	50–80	50–50	81.069	166.91	269.11	0.15463	2.37%
		30–30–30	80.886	166.68	268.96	0.15459	2.14%
		Linear	80.511	167.21	268.96	0.15455	1.67%
		Exponential	80.844	167.85	269.03	0.15554	2.09%
	Fully filled	50–50	80.907	167.21	269.52	0.15508	2.17%
		30–30–30	80.853	167.04	269.40	0.15507	2.10%
		Linear	80.454	167.47	269.23	0.15502	1.59%
		Exponential	80.916	169.12	270.13	0.15683	2.18%
X-type	50–80	50–50	81.003	167.38	269.43	0.15481	2.29%
		30–30–30	80.526	167.33	269.04	0.15479	1.69%
		Linear	80.962	167.22	269.31	0.15478	2.24%
		Exponential	80.885	168.03	269.17	0.15581	2.14%
	Fully filled	50–50	81.308	167.21	269.42	0.15539	2.67%
		30–30–30	80.841	167.01	269.22	0.15537	2.08%
		Linear	80.626	166.46	266.85	0.15534	1.81%
		Exponential	81.681	168.89	270.38	0.15669	3.14%
Octet-truss	50–80	50–50	80.469	167.28	269.12	0.15559	1.61%
		30–30–30	80.817	166.87	269.13	0.15562	2.05%
		Linear	80.763	166.78	269.02	0.15559	1.99%
		Exponential	81.566	168.39	270.02	0.15819	3.00%
	Fully filled	50–50	80.424	168.01	269.77	0.15714	1.56%
		30–30–30	80.675	167.09	269.28	0.15707	1.87%
		Linear	81.025	167.28	268.97	0.15707	2.32%
		Exponential	81.114	169.74	269.88	0.16115	2.43%

more separated mass over the blade essentially means that the thickness variation along the blade's span becomes more pronounced. This variation in thickness leads to a more significant change in the structural properties of the blade, particularly enhancing the stiffness toward the base. Moreover, the increased gradient constant causes a redistribution of the blade's mass, concentrating more material where it can effectively contribute to the stiffness without excessively increasing the overall weight. This balance between mass distribution and stiffness is critical in optimizing the blade's performance, ensuring that the structural integrity is maintained while achieving the desired vibrational characteristics. The base of the blade has a higher stiffness causing the blades to vibrate at a higher natural frequency.

The size of the lattice structures can have significant implications for the overall strength, stability, and fatigue life of the blade. When the lattices become very small due to a large gradient, it can potentially lead to localized stress concentrations. These stress concentrations can promote the initiation and propagation of cracks, which can ultimately lead to structural failure, particularly under cyclic loading conditions experienced during normal operation. Moreover, small lattice structures might also affect the material properties, such as stiffness and damping characteristics, which can further influence the dynamic behavior of the blade. Having very small lattices also have several benefits such as its flexibility. These structures are inherently compliant, meaning they can deform and flex under applied loads while maintaining structural integrity. This flexibility allows them to absorb and distribute mechanical stresses, making them suitable for applications requiring resilience and impact absorption. Therefore, while increasing the gradient may be desirable for certain reasons such as raising natural frequency, it's essential to carefully assess and mitigate the potential risks associated with small lattice sizes at the blade tip. This might involve strategies such as optimizing the lattice design, using advanced materials with enhanced fatigue resistance, or incorporating additional reinforcement or damping mechanisms to ensure the structural integrity and reliability of the blade under various operating conditions.

5. Multi-Lattices

A further research is toward multi-lattices because a singular lattice design may not adequately meet the specified requirements. For example, a conclusion reached in constant lattices is that the first natural frequency increases significantly while the higher modes of natural frequency remain relatively constant. From variable-based lattices, we set the lattices with the highest density at the root of the blade and the lowest relative density at the tip of blade. This ensures a good mass distribution to the blade. This also helps in increasing the natural frequency of higher modes when compared to hollow blade. Through multi-lattices, we can combine both advantages in constant and variable lattice designs. By selecting the highest frequency at the base of blade and lowest frequency of blade, we can find the design for location-based design, diamond, cubic; and full design, X-type, and octet-truss; which shows a higher frequency than the hollow blade.

An important factor in multi-lattice is the connection between two lattices. A combination of two or more minimal surfaces can be utilized to construct a lattice with multiple morphologies, allowing for a seamless transition. The mathematical definition of this transition can be either sharp or smooth. In the case of a smooth transition, an intermediary phase emerges, representing a hybrid between the employed minimal surfaces. A weighing function becomes instrumental in assigning distinct TPMS morphologies to various regions within the hybrid lattice. Yoo and Kim [20] and Yang et al. [21] have illustrated several instances of hybrid lattices and elucidated the underlying design methodology. A multi-morphology lattice of two topologies can be obtained via the following relation [14]:

$$\varphi_M = \gamma\varphi_{S1} + \left(1-\gamma\right)\varphi_{S2} \tag{14}$$

where φ_M is the multi-morphology lattice made of lattice φ_{S1} and lattice φ_{S2}, and γ is a spatial weighting function with a value between 0 and 1. γ can be described by a sigmoid function such that [21]:

$$\gamma\left(x,y,z\right) = \frac{1}{1+e^{kG\left(x,y,z\right)}} \tag{15}$$

where $G(x, y, z)$ represents a set of spatial coordinates defining the transition shape between two distinct regions of lattices, and k determines the width of that transition. In Figure 10, the sigmoid function is plotted in the z-direction using a number of k values. When k increases, the transitions decrease in length.

5.1. Multi-lattices Results

From the design, we are able to analyze up to four types of design. The results are shown in the Figure 11. The best design from both 50–80 and fully filled design from the previous two sections are chosen for analysis in this section. These four types of design are used to illustrate the important factor of using multiple lattices within a single blade.

When transitioning from a constant lattice design to a multi-lattice design paradigm, specifically when a particular lattice occupies 20% or less of the total blade, the introduction of two distinct types of lattices precipitates a notable decrease in the blade's first natural frequency (see Figure 11). This is because a constant lattice design typically maintains uniform stiffness throughout the blade; multi-lattice design creates a huge sudden decrease in stiffness characteristics notably when moving from a fully

FIGURE 10 Sigmoid function using different *k* values.

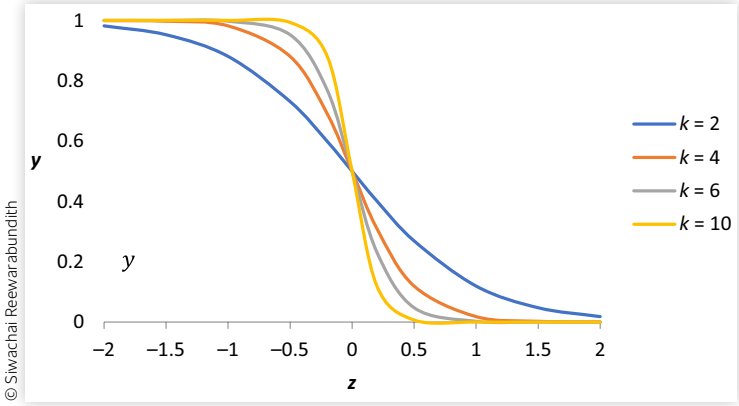

filled X-type to simple-cubic lattices. When the occupation of lower density lattices increases, the mass decreases and also the stiffness. This makes the transition section easy to break, resulting in lower natural frequency. Moreover, the examination of various combinations of multiple lattices yields a consistent pattern—a downward curve of first natural frequency characterized by minimal fluctuations between the 20% and 80% thresholds. However, there is a slight increase, or "bump," in the first natural frequency occurring at the 50% mark of lattice distribution. This finding suggests a complex interaction between the two lattice types, wherein a certain balance or midpoint may optimize vibrational characteristics. Yet, despite the findings, the introduction of multiple lattice types within a constant lattice framework may not yield favorable outcomes.

In contrast to the findings within constant lattice designs, the exploration of variable-based design reveals a different trend regarding first natural frequency dynamics when implementing multi-lattice configurations. The overarching pattern indicates a notable augmentation in the blade's first natural frequency, thereby suggesting an advantageous synergy between multiple lattice types. An intriguing observation surfaces when examining the distribution of this increase across varying percentages of lattice incorporation. Notably, at the 40% mark, the first natural frequency experiences its most substantial enhancement within the multi-lattice framework. This pattern signifies a critical threshold wherein the combined effect of two different lattice types creates the most pronounced improvement in vibrational characteristics. This means that the two types of lattice structures are well balanced, ensuring that all parts contribute to the stiffness of the blade without merely adding mass. The blade maximizes stiffness and minimizes unnecessary weight, leading to improved performance without compromising structural efficiency.

In contrast to the conventional single-lattice configuration, the optimal design for multi-lattices with *k* set as an example to 20 exhibits distinctive characteristics meaning that there should not be any transitions between two lattice structures. In a single-lattice structure, the natural frequency is primarily influenced by the inherent stiffness and mass of that singular lattice. However, in the multi-lattice scenario, the size of the lattices is precisely tailored to match the cavity space, resulting in a single row of lattice structures. This design choice using a high value of *k* minimizes the

FIGURE 11 Percentage of lattice space occupation versus first natural frequency in multi-lattices.

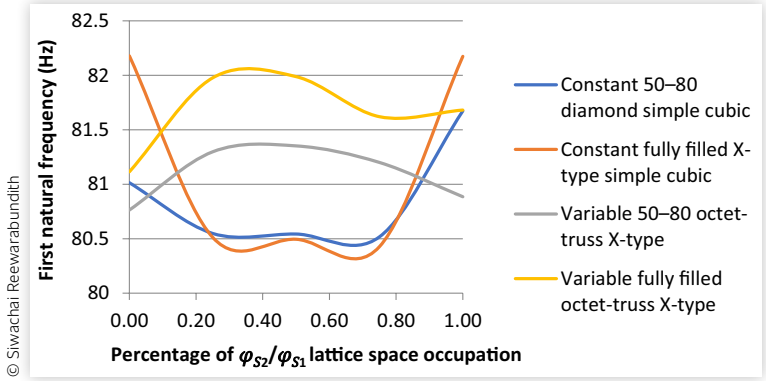

TABLE 8 Multi-lattice analytical results.

Configuration		k	Frequency mode			Mass
			Mode 1	Mode 2	Mode 3	
50–80 diamond simple-cubic	Constant	2	80.525	167.23	269.33	0.15456
		20	80.543	167.25	269.34	0.15447
50–80 octet-truss X-type	Exp	2	81.340	168.95	269.88	0.15821
		20	81.352	169.06	270.09	0.15805
Fully filled X-type simple-cubic	Constant	2	80.482	167.45	269.31	0.15516
		20	80.495	167.43	269.35	0.15509
Fully filled octet-truss X-type	Exp	2	81.840	169.80	270.88	0.16846
		20	81.988	170.24	271.56	0.16079

impact of transitions between lattices on the natural frequency, and in fact, there is a slight decrease in natural frequency due to the added mass during these transitions (see Table 8).

Comparatively, the single-lattice system lacks the complexity introduced by multiple lattice structures. The optimal multi-lattice design with $k = 20$ strategically leverages the interplay between lattice size, cavity space, and mass distribution to minimize changes in natural frequency during transitions. This underscores the nuanced trade-offs and advantages inherent in choosing a multi-lattice configuration over the more straightforward single-lattice counterpart. Even though some specific design for single-constant lattices may have a significant advantage in the first mode of natural frequency, multi-lattices use the combination of multiple lattices and gradient-based lattices, converging both ideas to ensure that all the modes of natural frequency will have an improvement, therefore satisfying the requirements of this research.

6. Experimental Verification

The three types of blades being analyzed are the hollow blade, 50–80 location-based, and fully filled exponential X-type + octet-truss lattice blade. These blades are the results of the previous section and are produced using additive manufacturing techniques. To correlate the experimental studies with the numerical results presented earlier, we conducted modal testing to determine the experimental modal parameters. The setup is shown in Figure 12. The experimental apparatus includes 3D-printed blades, bolts, Sirius 8-channel vibration analyzer, modal hammer, weighing scale, accelerometer, and Dewesoft modal software. The foundation of the blade is connected to the fixed support of the table through the use of bolts, 16 measurement points of the blade are mapped into Dewesoft software, which are used to recreate the mode shapes in the modal analysis section after the modal testing. The points are distanced at 40 mm in the

FIGURE 12 Modal analysis experiment setup.

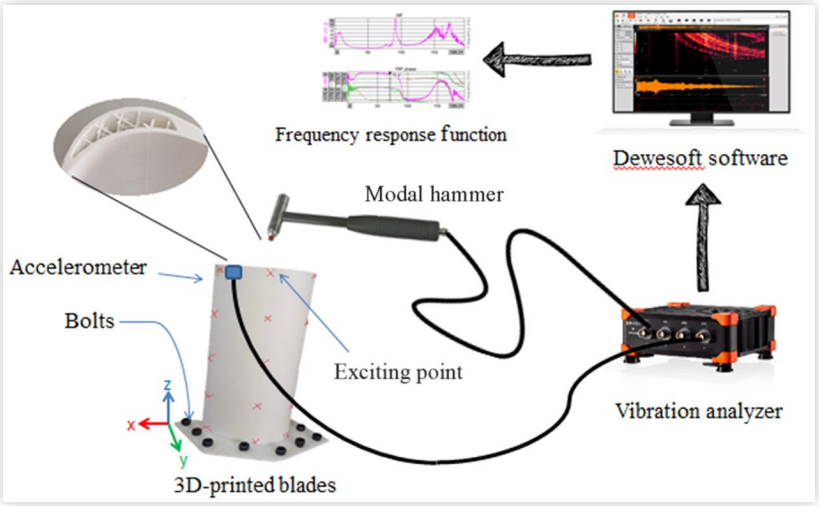

FIGURE 13 50–80 exponential X-type + octet-truss FRF.

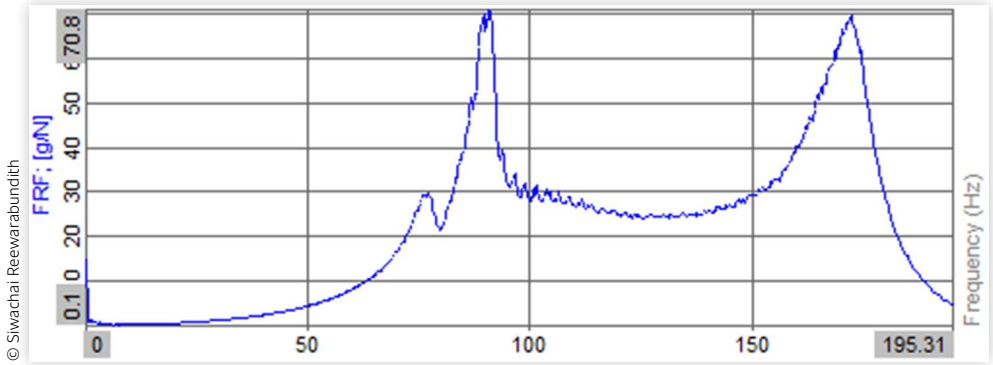

y-direction and 54 mm in the z-direction. The bottom nodes are distanced at 5 mm from the base.

The method employed is a single-input single-output (SISO) test. The frequency range is set between 0 Hz and 400 Hz, with a sampling rate of 1024 samples per second and spectral lines at 1024 Hz. During impact testing, a modal hammer with a rubber tip is used to strike the free end of the blade with a force of 1 N, inducing vibrations in the blade, The window configuration for this test is set to force, and a second hit trigger warning is implemented to avoid double hits during each round of strikes. The modal hammer strikes each of the 16 nodal points, with data being averaged over four hits as shown in red cross in Figure 12. Simultaneously, an accelerometer is affixed to the trailing edge of the blade close to the nodal point. Its output, in the form of electrical signals, processed and interpreted by Dewesoft software, providing a visual representation of the blade's natural frequencies. The results are displayed on a computer screen in the form of a frequency response function (FRF) for each nodal point. Each frequency response is added to form the final FRF.

By matching the natural frequencies obtained from the experiment with the numerical modal analysis predictions, we could confirm the accuracy of our numerical models carried out using ANSYS Modal Analysis software. This comparison revealed that the numerical models were reliable and could be used to predict the performance of different lattice configurations. The FRF results shown in Figures 13 and 14 shows that for 50–80-based lattices, there is a 15% increase in the first natural frequency and a 14.6% increase in the second natural frequency when compared to the experimental hollow blade. There is a 6% difference error with the numerical computation for the first natural frequency and 2.3% difference in the second natural frequency. Whereas for the full-based lattices, there is a 9.4% increase in the first natural frequency and a 12.7% increase in the second natural frequency. The difference error is around 5.1% for the first natural frequency and 0.4% in the second natural frequency compared to the numerical analysis (see Table 9).

From mode shapes, we can find the displacement distribution of the blade at the first and second modes of natural frequency. The first mode is the bending mode and the second mode is a torsional mode. Nodes are points where the amplitude is minimum, and anti-node points where the amplitude is maximum can be seen clearly in Figures 15, 16, and 17. The node in the first mode is generated at the root of the blade where it is fixed as a support, while the anti-node is present at the trailing edge of the shroud side. Whereas for the second mode, the blade bends inward. It can be seen that lattice structures reduce the overall displacement for two modes. Regarding structural stress, most of the stress is concentrated at the supports, particularly at the root where the

FIGURE 14 Fully filled exponential X-type + octet-truss FRF.

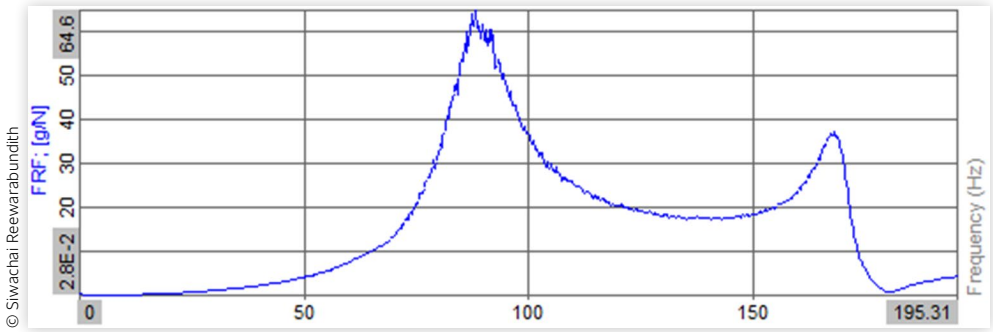

TABLE 9 Experiment results of 3D-printed blades.

Configuration		Mass (kg)	1st mode	2nd mode
Hollow	Computation	0.15408	79.191	147.90
	Experiment	0.14410	78.300	158.70
50–80 Exp X-type + octet-truss	Computation	0.15841	85.298	169.02
	Experiment	0.14690	90.820	172.85
Fully filled Exp X-type + octet-truss	Computation	0.16079	81.517	169.15
	Experiment	0.14770	85.690	169.95

FIGURE 15 First (left) and second (right) mode shapes of 50–80 exponential X-type + octet-truss.

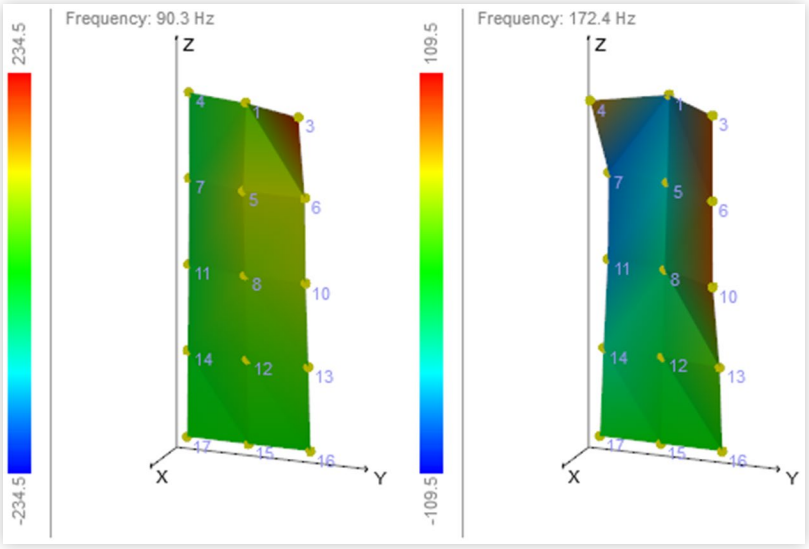

FIGURE 16 First (left) and second (right) mode shapes of fully filled exponential X-type + octet-truss.

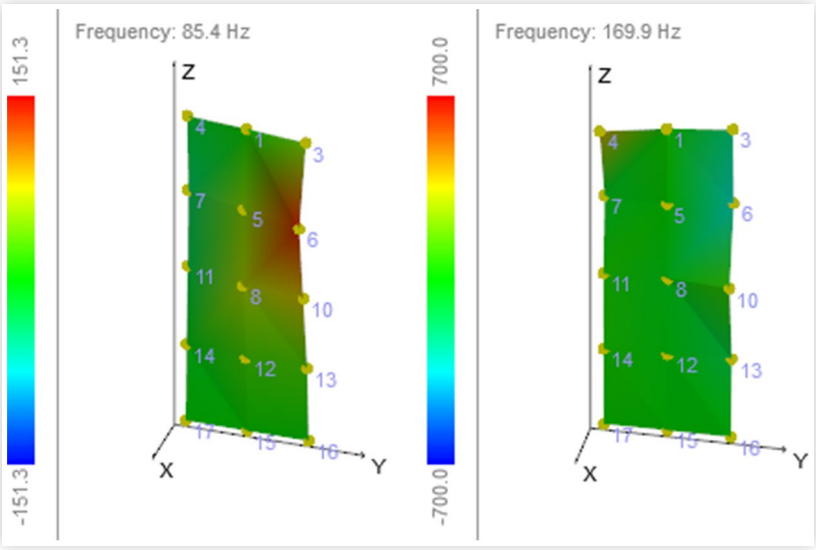

FIGURE 17 First (left) and second (right) mode shapes of hollow blade.

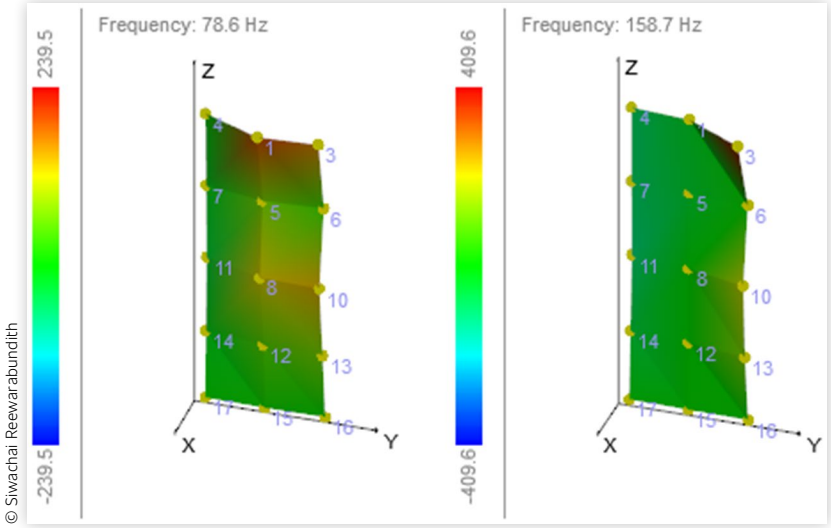

blade is fixed and subjected to high loads. As the lattice structures are used within the blade, they help reduce the stress throughout the structure. The lattice design effectively lowers the overall stress within the blade by redistributing forces and reinforcing areas prone to higher loads. As a result, the stresses in the blade are significantly reduced, leading to less deflection of the blade shown in the figures for improved performance and durability of both the blade and the lattice structure. This stress reduction is critical for preventing structural failure and ensuring the blade can withstand operational loads efficiently.

The variance in error observed within our calculations could potentially be attributed to multiple factors starting from the assumptions we make during our analysis. It's crucial to recognize that while numerical analysis serves as a valuable tool in understanding complex systems, they often operate under simplifying assumptions that may not fully encapsulate the intricacies of real-world conditions. This discrepancy between theoretical models and practical realities can manifest itself in various ways, leading to deviations from expected outcomes. One of the primary simplifications commonly employed in numerical analysis is the assumption of linear vibration. While this assumption greatly simplifies the mathematical models used in our calculations, it inherently neglects the nonlinear behavior that may occur in real-world systems. Nonlinear effects can arise due to a variety of factors, such as material properties, geometrical irregularities, and dynamic interactions between components. These nonlinearities can significantly impact the system's response and exhibit complex behaviors such as frequency-dependent stiffness, amplitude-dependent damping, and even chaotic responses, potentially leading to discrepancies between predicted and observed behavior.

7. Conclusions

In conclusion, constant lattice designs are more important in the first mode of natural frequency and the critical point, identified at a thickness of 0.5 mm in the constant lattice analysis, may exhibit a distinctive trend within the context of lattice structures. The gradient-based designs are more likely to impact significantly as the modes increases. Multi-lattices involve selecting the best design in both constant and variable lattice design, which results in further improvement in all modes of natural frequencies. The results demonstrate that location-based 50–80 exponential-based lattice structures combining octet-truss and X-type lattices yield the best performance, achieving a 15% increase in the first mode and 14.6% in the second mode when compared to hollow blade, respectively. In comparison, fully infilled 50–80 exponential-based lattice structures with a combination of octet-truss and X-type lattices achieve a 9.4% increase in the first mode and 12.7% in the second mode, respectively. This analysis is useful when optimizing the lattices within blades to ensure the highest natural frequency, not only for the first modes but also for the higher modes of frequency. Whether considering a constant lattice, variable thickness lattices, or multi-lattices with specific configurations, the intricate balance of factors such as thickness, number of sections, and transition effects plays a pivotal role in shaping the overall performance of lattice structures in dynamic scenarios.

Contact Information

Siwachai Reewarabundith
rhugo2010@gmail.com

References

1. Soares, C., "Gas Turbines: An Introduction and Applications," in Soares, C. (Ed.), *Gas Turbines* (Elsevier: Butterworth-Heinemann, 2008), 1-31, ISBN 9780750679695, https://doi.org/10.1016/B978-075067969-5.50006-5.
2. Hodson, H.P. and Howell, R.J., "The Role of Transition in High-Lift Low-Pressure Turbines for Aeroengines," *Progress in Aerospace Sciences* 41, no. 6 (2005): 419-454.
3. Wisler, D., "The Technical and Economic Relevance of Understanding Blade Row Interactions Effects in Turbomachinery," von Karman Institute for Fluid Dynamics Lecture Series 1998-02, 1998.
4. Carlos, M., "New Technology Used in Gas Turbine Blade Materials," *Scientia Et Technica* 1, no. 36 (2007): 297-301.
5. Feig, P.D., "Revolutionary Opportunities for Materials and Structures Study, Addendum," Aircraft Propulsion and Power, Addendum - NASA Technical Reports Server (NTRS), 1987.
6. Ewins, D.J., "Control of Vibration and Resonance in Aero Engines and Rotating Machinery – An Overview," *International Journal of Pressure Vessels and Piping* 87, no. 9 (2010): 504-510.
7. Arts T., "Aerodynamic Performance of Two Very High Lift Low Pressure Turbine Airfoils (T106c – T2) At Low Reynolds and High Mach Numbers," in *5th European Conference for Aeronautics and Space Sciences (EUCASS)*, Munich, Germany, 2013.
8. Srinivasan, A.V., "Flutter and Resonant Vibration Characteristics of Engine Blades: An IGTI Scholar Paper," in *Proceedings of the ASME 1997 International Gas Turbine and Aeroengine Congress and Exhibition*, Vol. 4, Manufacturing Materials and Metallurgy; Ceramics; Structures and Dynamics; Controls, Diagnostics and Instrumentation; Education; IGTI Scholar Award. Orlando, Florida, USA. June 2–5, 1997, V004T17A001, ASME, https://doi.org/10.1115/97-GT-533.
9. Binder, A., Schröder, T., and Hourmouziadis, J., "Turbulence Measurements in a Multistage Low Pressure Turbine," *ASME Journal of Turbomachinery* 111 (1989): 153-161.
10. Maconachie, T., Leary, M., Lozanovski, B. et al., "SLM Lattice Structures: Properties, Performance, Applications and Challenges," *Materials and Design* 183 (2019): 108137.
11. Gibson, L.J., "Modelling the Mechanical Behavior of Cellular Materials," *Materials Science and Engineering: A* 110 (1989): 1-36.
12. Ashby, G. and Casale, M., "Empirical Dissociations between Rule-Based and Similarity-Based Categorization," *Behavioral and Brain Sciences* 28, no. 1 (2005): 15-16.
13. Zargarian, A., Esfahanian, M., Kadkhodapour, J. et al., "On the Fatigue Behavior of Additive Manufactured Lattice Structures," *Theoretical and Applied Fracture Mechanics* 100 (2019): 225-232.
14. Hussain, S., Ghopa, W.A.W., Singh, S., Azman, A.H. et al., "Comparison of Lattice Structure Configurations for Suitability in Turbine Blades Using Modal and Harmonic Response Analysis," in Abdullah, S., Karam Singh, S.S., and Md Nor, N. (Eds), *Structural Integrity Cases in Mechanical and Civil Engineering. SDMMS 2020*, Structural Integrity, vol. 23 (Cham: Springer, 2022), doi:https://doi.org/10.1007/978-3-030-85646-5_5.
15. El-Sayed, M.A., Essa, K., Ghazy, M. et al., "Design Optimization of Additively Manufactured Titanium Lattice Structures for Biomedical Implants," *International Journal of Advanced Manufacturing Technology* 110 (2020): 2257-2268, doi:https://doi.org/10.1007/s00170-020-05982-8.
16. Xiao, L., Xu, X., Song, W. et al., "A Multi-Cell Hybrid Approach to Elevate the Energy Absorption of Micro-Lattice Materials," *Materials (Basel, Switzerland)* 13 (2020): 4083, doi:10.3390/ma13184083.
17. Wang, Y., Feng, C., Zhang, Z. et al., "Compressive Property of Additively-Manufactured Micro-Architectures with X-Type Lattice Unit Cell," *Materials* 15 (2022): 3815, doi:https://doi.org/10.3390/ma15113815.
18. Hillewaert, K. and Cagnone, J.S., "CS2 - Spanwise Periodic DNS/LES of the Transitional Flow in T106 LP Turbine Cascades," in *5th International Workshop on High-Order CFD Methods*, Argo Group, Cenaero, Kissimmee, Florida, 2017.
19. Antorkas, S., Montomoli, F., and Massini, M., "Topology Optimization of Gas Turbine Blades for Additive Manufacturing," in *Proceedings of Global Power and Propulsion Society*, Chania, Greece, 2020.
20. Yoo, D.J. and Kim, K.H., "An Advanced Multi-Morphology Porous Scaffold Design Method Using Volumetric Distance Field and Beta Growth Function," *International Journal of Precision Engineering and Manufacturing* 16, no. 9 (2015): 2021-2032.
21. Yang, N., Quan, Z., Zhang, D. et al., "Multi-Morphology Transition Hybridization Cad Design of Minimal Surface Porous Structures for use in Tissue Engineering," *Computer-Aided Design* 56 (2014): 11-21, doi:https://doi.org/10.1016/j.cad.2014.06.006.